The Astrophysical Journal, 593:587–596, 2003 August 10

LOSS CONE PRECURSORS TO FORBUSH DECREASES AND ADVANCE WARNING OF SPACE WEATHER EFFECTS

K. Leerungnavarat and D. Ruffolo
Department of Physics, Chulalongkorn University, Bangkok 10330, Thailand

and

J. W. Bieber
Bartol Research Institute, University of Delaware, Newark, DE 19716
Received 2003 January 14; accepted 2003 April 14

ABSTRACT

Ground-based observations of cosmic rays by neutron monitors and muon detectors have found precursor anisotropies before the arrival of an interplanetary shock and subsequent Forbush decrease, possibly providing advance warning of space weather effects on shock impact at the Earth's magnetosphere. Surprisingly, muon detectors observe precursors with a greater lead time than neutron monitors. Here, we explain both loss cone and shock reflection precursors in a common mathematical framework and perform time-dependent numerical simulations of cosmic-ray transport near an oblique, planar shock. We examine parameters of loss cone precursors as a function of the shock–magnetic field angle and q, the spectral index of magnetic turbulence. More energetic particles correspond to a lower value of q and a higher value of λ, the interplanetary scattering mean free path. We conclude that loss cones should typically be detectable 4 hr prior to shock arrival at neutron monitor energies ($\sim$10 GeV) and 15 hr prior to shock arrival at muon detector energies ($\sim$30 GeV). In addition, the angular width of the loss cone provides a potential method of forecasting the shock-field angle, as the predicted width is substantially larger for quasi-parallel shocks than for quasi-perpendicular shocks, leading to a better indication of the shock arrival time.

Subject headings: cosmic rays — interplanetary medium — shock waves — solar-terrestrial relations

1. INTRODUCTION

An important aspect of space weather prediction is to determine whether or not an interplanetary shock is headed toward the Earth and at approximately what time its impact is expected. While the relationship between coronal mass ejections (CMEs) and Forbush decreases in Galactic cosmic rays is now well established (Cane 1993; Cane et al. 1994; Cane, Richardson, & von Rosenvinge 1996), it is less generally recognized that cosmic-ray decreases are often accompanied by strong enhancements of the cosmic-ray anisotropy (Lockwood 1971; Duggal & Pomerantz 1976; Nagashima et al. 1992), some of which extend into the region upstream of the approaching shock. Such precursory anisotropies provide a key mechanism by which information about the presence of a disturbance can be transmitted to remote locations upstream of the shock. Because cosmic rays are fast and have large scattering mean free paths ($\sim$1 AU) in the solar wind, this information travels rapidly and may prove useful for space weather forecasting.

Precursory anisotropies have generally been interpreted as kinetic effects related to interaction of ambient cosmic rays with the approaching shock (Nagashima, Fujimoto, & Morishita 1994; Belov et al. 1995; Morishita et al. 1997; Bieber & Evenson 1998; Ruffolo et al. 1999). Measurements of cosmic rays by ground-based detection of atmospheric secondary neutrons or muons have proved to provide our most accurate information on the directional distribution of cosmic rays, routinely monitoring the anisotropy to a resolution of 0.1% (the average quiet-time anisotropy is about 0.7%; Chen & Bieber 1993). Precursory decreases apparently result from a "loss cone" effect, in which a neutron monitor station or muon detector is magnetically connected to the cosmic ray–depleted region downstream of the shock. Precursory increases apparently result from particles reflecting from the approaching shock (Dorman, Iucci, & Villoresi 1995).

The potential for neutron monitors to contribute to space weather forecasting is also indicated by statistical results of Kudela et al. (1995, 1997), who found correlations at the 40% level between cosmic-ray "fluctuations" recorded by neutron monitors and the D_{ST} value measured $\sim$10 hr later. The source of the effect could be precursory anisotropy, because anisotropy is manifested as enhanced variability in single-station data.

Figure 1 displays results from two surveys of cosmic-ray precursors conducted with ground-based instrumentation. Each histogram displays the lead time of the precursor relative to the storm sudden commencement (SSC) associated with the CME shock. The upper histogram is for 14 "major" geomagnetic storms surveyed with a network of neutron monitors (Belov et al. 2001). These major storms are simply the ones identified by Gosling et al. (1990) with a peak Kp index of 8− or greater. The lower histogram is for 22 "large" geomagnetic storms surveyed with surface muon telescopes (Munakata et al. 2000). A large storm is defined as one for which the peak Kp index was 7− or greater. Note that both neutron monitors and muon detectors measure the intensity of secondary particles produced by interactions of primary cosmic rays, mostly protons, with atoms in Earth's atmosphere. The typical primary cosmic-ray energy producing the secondaries modulated by Forbush decreases is $\sim$10 GeV for neutron monitors and $\sim$30 GeV for muon detectors.

The precursors marked "LC" in the histograms are those that displayed clear characteristics of a loss cone, i.e.,

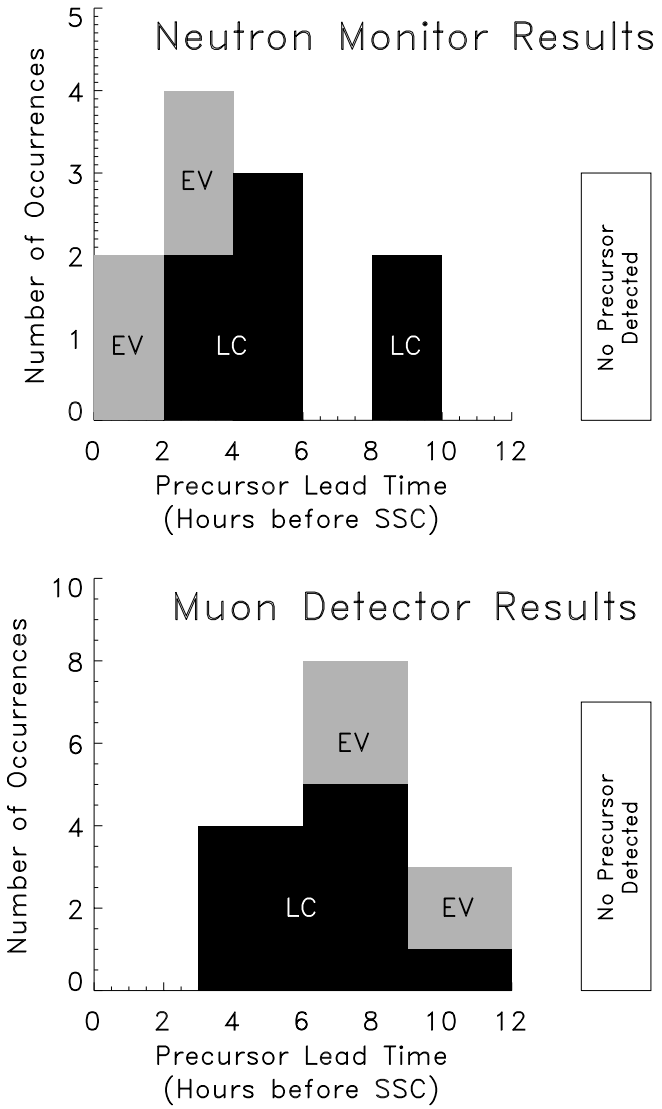

FIG. 1.—Occurrence histograms showing when a shock precursor was first observed relative to the associated SSC. Top and bottom histograms show results of surveys conducted with neutron monitors (Belov et al. 2001) and muon detectors (Munakata et al. 2000), respectively. "LC" and "EV" denote loss cone and enhanced variance precursors (see text).

suppressed intensities of particles moving antisunward along the local magnetic field line. The precursors marked "EV" (enhanced variance) are similar but are not as clearly aligned with the magnetic field. There are several possible explanations for the EV-type precursor. First, they could be loss cones observed in situations in which the locally measured magnetic field is not representative of the large-scale field sampled by the particles. These particles have Larmor radii of ~0.05–0.1 AU, which is comparable to the correlation length of interplanetary magnetic turbulence. It is thus plausible that the local field at the observation point could deviate substantially from the field averaged over the particle orbit. Second, the EV precursors could be loss cones observed from a moving reference frame. Theoretical results presented below suggest that upstream anisotropies will be axisymmetric with respect to the large-scale field when viewed in the de Hoffman–Teller frame of the shock. The observations presented in Figure 1, however, were made in an Earth-fixed frame. Future observational studies should examine whether EV precursors can be transformed into clear loss cones by means of a suitable change of reference frame. Finally, the EV precursors may represent anisotropies that really are not field-aligned, such as the $\boldsymbol{B} \times \nabla n$ drift anisotropy (Bieber & Evenson 1998).

Figure 1 shows, first, that precursors accompany the majority of large or major geomagnetic storms. The muon detectors observed precursors in 15 of 22 large storms (68%), while the neutron monitors observed precursors in 11 of 14 major storms (79%). As discussed by Munakata et al. (2000), if the muon detector survey is limited to the largest storms in the sample (peak Kp of 8 or greater), then the proportion with identified precursors rises to eight of nine (89%). The figure shows, second, that the lead time of precursors relative to the SSC is typically several hours and can be as much as 12 hr. This is enough to be useful for space weather forecasting, as it provides substantially longer advance warning than the 0.5–1 hr lead time provided by direct shock detection at a spacecraft stationed at the upstream Sun-Earth Lagrangian point.

Finally, Figure 1 documents a clear difference between the lead times provided by muon detectors and neutron monitors. Typical lead times are 8 hr for muon detectors and 4 hr for neutron monitors. This result is rather surprising, because the Forbush decrease following the shock is typically deeper at the lower energies measured by neutron monitors. It thus seems natural to expect that loss cone particles escaping into the upstream region from the depleted region downstream of the shock would be more readily detected at the lower energies, the opposite of what is observed.

We propose to explain the difference in lead times in terms of the difference in primary cosmic-ray energy to which neutron monitors and muon detectors are sensitive and the different interplanetary magnetic power spectra and scattering mean free paths that apply at those energies. Figure 2 shows a representative power spectrum of interplanetary magnetic

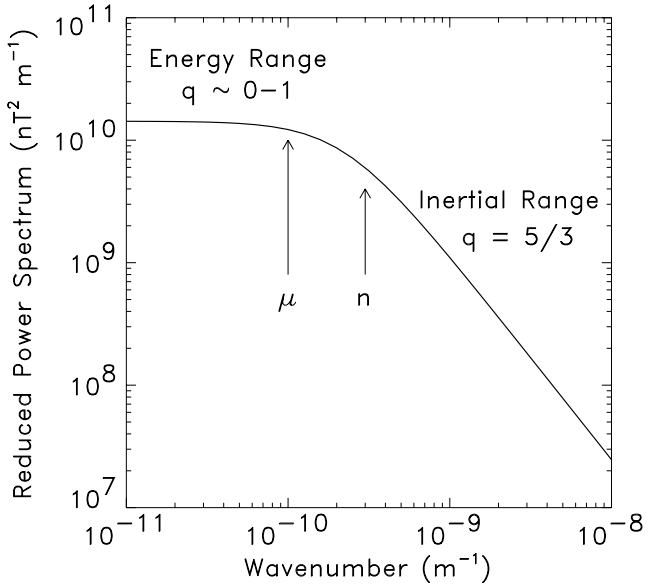

FIG. 2.—Representative power spectrum of interplanetary magnetic turbulence, showing typical resonant wavenumbers for neutron monitor energies ("n") and muon detector energies ("μ"). The neutron monitor resonance is almost exactly at the turbulence correlation scale, $k = \lambda_c^{-1} \approx 3 \times 10^{-10}$ m^{-1}. The model spectrum is from eq. (13) of Bieber et al. (1994).

turbulence, including typical resonant wavenumbers for primary cosmic rays detected by means of atmospheric secondary neutrons ("n") or muons ("μ"). Figure 2 was obtained from survey observations of interplanetary magnetic spectra (Bieber et al. 1994 and references therein). We think it is reasonable to use this spectrum for our purposes, because any upstream waves excited by the shock would be at wavenumbers much higher than the resonant wavenumbers of the cosmic rays of interest here. On the other hand, it should be recognized that the actual spectrum at any given time can vary considerably from the average spectrum, which may be one factor contributing to the large spread of precursor lead times displayed in Figure 1.

Because the typical resonances for neutron monitor and muon detector primaries are in the transition region between energy range and inertial range behavior, the local power-law index varies comparatively rapidly with wavenumber k. This power-law index q of the reduced power spectrum as a function of wavenumber is well known to affect the transport of cosmic rays (Jokipii 1966). Here we point out that cosmic rays of $\sim$30 GeV, to which a muon detector is sensitive, experience a substantially lower q-value than cosmic rays at $\sim$10 GeV, as measured by neutron monitors, and we examine the expected influence of q on the lead time using the theoretical framework of Ruffolo (1999).

In the present work, we show that precursors to Forbush decreases (both loss cone decreases and shock reflection increases) can be described in a common mathematical framework based on a pitch-angle transport equation. Using time-dependent numerical simulations of the particle transport near a planar shock, we can indeed explain the increased lead time for muon detector versus neutron monitor observations in terms of the different mean free path λ and spectral index of interplanetary turbulence q at the relevant wavenumber range. We point out the potential for observations of loss cone precursors to provide advance warning of the onset of space weather effects at Earth and examine how the shock geometry and q affect the angular width of the loss cone precursor and the length scale over which it can be observed.

2. MODEL

2.1. *Transport Equation*

The strong anisotropies in Galactic cosmic rays that are observed shortly before the impact of an interplanetary shock are clearly outside the framework of diffusive transport. We can make substantial progress in understanding these observed effects of an interplanetary shock on the distribution of energetic charged particles by numerically solving a Fokker-Planck equation of transport that includes the effects of interplanetary scattering and solar wind convection to first order in the solar wind speed (Ruffolo 1995) and by incorporating the changes in pitch angle and momentum as a particle crosses or is reflected by an oblique shock, i.e., a shock oriented at an arbitrary angle with respect to the mean magnetic field.

It turns out that both precursory increases and precursory decreases can be interpreted in terms of a simple model of an oblique, plane-parallel shock with straight magnetic field lines on either side (Ruffolo 1999). Consider the de Hoffmann–Teller reference frame, in which the shock is stationary, the fluid flow is parallel to the magnetic field, and the electric field is zero (de Hoffmann & Teller 1950). In this reference frame, the first-order Fermi and shock drift mechanisms are combined into a single mathematical framework. The pitch-angle transport equation simplifies to

$$\frac{\partial F}{\partial t} = -\frac{\partial}{\partial z}\left[\mu v + \left(1-\mu^2\frac{v^2}{c^2}\right)u\right]F + \frac{\partial}{\partial \mu}\left[\frac{\varphi}{2}\frac{\partial}{\partial \mu}\left(1-\mu\frac{uv}{c^2}\right)F\right], \quad (1)$$

where $F(t,z,\mu,p) \equiv d^3N/(dz\,d\mu\,dp)$ is the distribution function of particles in a magnetic flux tube, t is the time in the shock (de Hoffmann–Teller) frame, z is the distance from the shock along the magnetic field in the shock frame, μ is the cosine of the pitch angle in the local fluid frame (the pitch angle is the angle between the particle velocity and the local magnetic field), p is the momentum in the local fluid frame, v is the particle speed in the local fluid frame, $u = u_n \sec\theta_{Bn}$ is the fluid speed along the field relative to the shock, u_n is the fluid speed normal to the shock, θ_{Bn} is the angle between the magnetic field and the shock normal, and $\varphi(\mu)$ is the pitch-angle scattering coefficient. A similar transport equation was employed by Kirk & Schneider (1987) to study ultrarelativistic particle acceleration and by Kirk (1988) to examine the effect of the form of $\varphi(\mu)$. In the present work, the sign conventions for z and μ are as follows: z increases toward the upstream direction, $z > 0$ for locations upstream of the shock (outward from the Sun, in the case of a Forbush decrease), and $z < 0$ for locations downstream of the shock. Similarly, $\mu > 0$ for motion in the upstream direction in the fluid frame. For consistency with the above we have $u < 0$, i.e., fluid flow from upstream to downstream in the shock frame.

We use the following form of the pitch-angle scattering coefficient:

$$\varphi(\mu) = A|\mu|^{q-1}(1-\mu^2) \quad (2)$$

(Jokipii 1971), where the parameter A can be related to λ, the parallel mean free path for interplanetary scattering, by the well-known expression

$$\frac{v}{A} = \frac{(2-q)(4-q)}{3}\lambda, \quad (3)$$

and q characterizes the steepness of a presumed power spectrum of interplanetary magnetic turbulence varying with wavenumber k as $|k|^{-q}$. In equation (2), a value of $q < 1$ leads to enhanced pitch-angle diffusion at $\mu = 0$ (a pitch angle of 90°) and a flatter pitch-angle distribution near $\mu = 0$, whereas $q > 1$ leads to less pitch-angle diffusion and a steeper gradient of the pitch-angle distribution near $\mu = 0$. Since the observed power spectrum is typically similar to that shown in Figure 2, with an effective spectral index q that varies with wavenumber and hence with particle energy, we perform simulations of cosmic-ray pitch-angle transport near a shock for various values of q.

2.2. *Steady State Separable Solutions*

A detailed study of Forbush decrease precursors requires time-dependent numerical simulations using a pitch-angle transport equation, as described above, for which solutions are shown in § 3. On the other hand, much insight into these solutions can be gained by examining the steady state

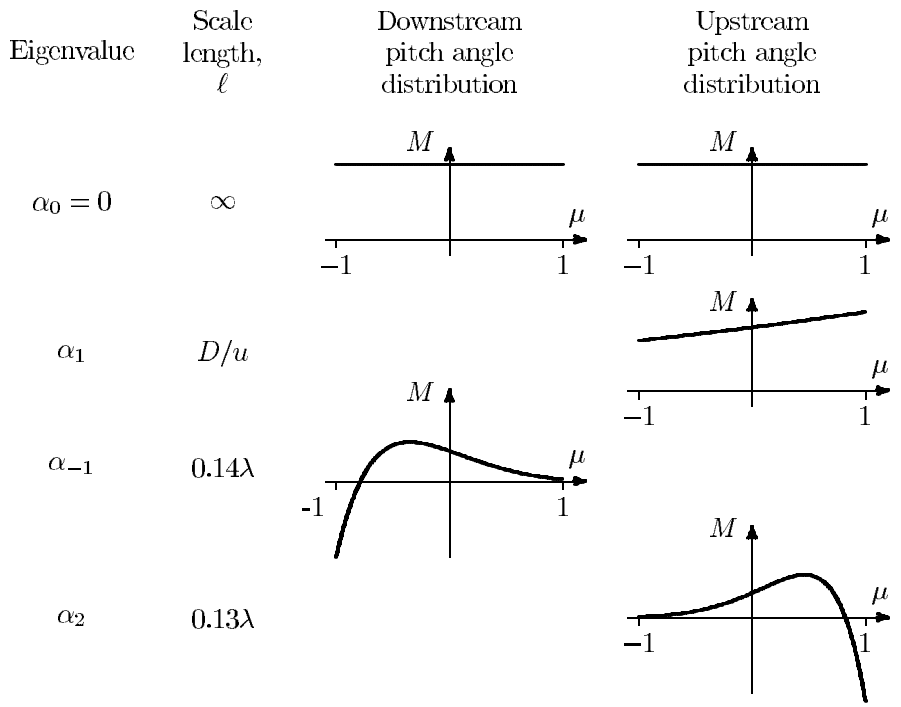

FIG. 3.—Separable solutions of the transport equation in the steady state on the downstream and upstream sides of a shock at $z = 0$ for $q = 1$. The quantity μ represents the cosine of the pitch angle. For each solution, $F_w = e^{\pm z/\ell} M(\mu)$, so ℓ represents the scale length over which the solution decays upstream or downstream of the shock. $D = v\lambda/3$ is the spatial diffusion coefficient.

problem, which is amenable to analysis in terms of separable solutions (Fig. 3), although finding the amplitudes of the solutions requires a numerical solution of the full transport equation (Ruffolo 1999). The low-order solutions, at long distance scales from the shock, are found in the diffusion approximation (see, e.g., Krymskii 1977) and constitute the "standard" solution of the particle distribution function for a planar shock. In addition, we point out that higher order solutions appear at shorter distance scales from an oblique shock. The loss cone precursor is such a solution and can flag an observer to the imminent approach of an interplanetary shock.

We should point out at the outset that this problem has only one length scale, λ. Mathematically, this implies that all lengths can be expressed in terms of λ. Physically, it implies that the decay lengths and lead times of precursor features will be directly proportional to the mean free path.

Following Kirk & Schneider (1987), in the steady state it is possible to find separable solutions if we restrict the z-domain to only one side of the shock. We set $\partial F/\partial t = 0$ and $F_w = (1 - \mu u v/c^2)F$ as the distribution function in the fluid frame and use the separation of variables, $F_w(\mu, z) = M(\mu)Z(z)$, yielding $Z \propto e^{\pm z/\ell}$ for a (positive) decay length ℓ and

$$\frac{\partial}{\partial \mu}\left[(1-\mu^2)|\mu|^{q-1}\frac{\partial M}{\partial \mu}\right] - \alpha\left(\mu + \frac{u}{v}\right)M = 0 \,, \qquad (4)$$

where $\alpha \equiv \pm 2v/(A\ell)$ is a (discrete) eigenvalue of the equation. To avoid divergence as $z \to \pm\infty$, $\alpha = 2v/(A\ell)$ applies downstream ($z < 0$) and $\alpha = -2v/(A\ell)$ upstream. Following Ruffolo (1999), these are labeled α_i, with a positive index i for upstream solutions. Note that $\alpha_0 = 0$ corresponds to a separable solution that is constant in μ and z and can be found either upstream or downstream. For q- and u/v-values of interest, eigenvalues and eigenfunctions were evaluated by using the Mathematica software package (Wolfram Research, Inc.).

Figure 3 shows pitch-angle distributions for low-order separable solutions on either side of the shock for $q = 1$ and $|u_n| \sec\theta_{Bn}/v = 0.075$. The α_0 and α_1 solutions correspond to the solutions in the diffusive approximation (see, e.g., Krymskii 1977), while higher order separable solutions appear closer to the shock. Note that the eigenfunctions $M(\mu)$ satisfy an orthogonality relation,

$$\int_{-1}^{1} M_i(\mu)M_j(\mu)(\mu v + u)\,d\mu = A_i\delta_{ij} \,, \qquad (5)$$

where A_i is a constant and $\mu v + u$ represents the streaming+convection speed for each μ. In particular, orthogonality with the constant solution implies that each nonconstant eigenfunction has zero net (streaming+convection) flux. The α_2 solution leads to upstream precursor features, i.e., a loss cone deficit at μ close to 1 (pitch angle close to zero) and a reflection-related increase at lower positive μ, balanced for zero net spatial flux. Thus, we predict that these features should always appear in tandem. Since we find the loss cone feature to be more easily recognized in the data, and thus more useful as an indicator of impending space weather disturbances, we simply refer to this solution as the loss cone precursor.

An important characteristic of the separable solutions, including the α_2 loss cone feature, is their decay with distance z from the shock along the field according to $e^{\pm z/\ell}$,

TABLE 1
DECAY LENGTH OF THE LOSS CONE FEATURE IN A STEADY STATE

q	ℓ_2^0/λ	β_2
0.1	0.240	2.52
0.5	0.195	2.40
1.0	0.138	2.34
1.5	0.073	2.37

NOTE.—The decay length is given by $\ell_2 = \ell_2^0/(1 + \beta_2|u_n| \sec\theta_{Bn}/v)$.

with a different decay length ℓ_i for each solution, given by

$$\ell_i = \frac{2}{|\alpha_i|}\frac{v}{A} = \frac{2(2-q)(4-q)}{3|\alpha_i|}\lambda\ . \tag{6}$$

From Mathematica calculations of α_i, we have found the decay length to be well approximated by

$$\ell_i \approx \frac{\ell_i^0}{1 \pm \beta_i|u|/v} = \frac{\ell_i^0}{1 \pm \beta_i|u_n| \sec\theta_{Bn}/v}\ , \tag{7}$$

where β_i is a constant between 2.2 and 2.6 and the "plus/minus" sign follows the sign of i.

Table 1 shows the values of ℓ_2^0 and β_2 corresponding to various values of the magnetic fluctuation power-law index q. Note the systematic increase in the decay length with decreasing q, which helps explain why measuring more energetic cosmic rays can provide more advanced warning of the onset of space weather effects (see Fig. 2). The increasing mean free path with increasing energy is another important factor.

In summary, the steady state solutions serve to classify the behavior of the cosmic-ray distribution function near a shock; in particular, the α_2 component, an upstream precursor, includes the loss cone feature as well as a reflection-related increase, balanced for zero net spatial flux, both of which have been observed by ground-based neutron monitors. This solution decays exponentially with distance upstream of the shock, with a decay length that strongly depends on the turbulence index q and hence the particle energy. In the full transport simulations, we find qualitatively similar behavior, but with quantitatively different decay lengths that are determined numerically.

2.3. *Numerical Simulations*

We model upstream precursors of Forbush decreases by solving equation (1) for the time-dependent distribution of Galactic cosmic rays near an oblique, interplanetary shock. Physically, we consider that Forbush decreases downstream of a shock result because the fresh downstream plasma emitted along with a CME has a relatively low density of Galactic cosmic rays, and their flow into this downstream plasma is inhibited by particle reflection at the shock. (Our particle orbit simulations show that even for a magnetic compression ratio as low as 1.5, a majority of energetic particles coming from upstream are reflected.) Therefore, we assume that the particle distribution function is initially constant with a constant inflow upstream and initially constant at half that density downstream.

We performed time-dependent simulations of Galactic cosmic rays with varying magnetic field–shock angles and q, considering protons with a momentum of $p = 25$ GeV c^{-1}. For highly relativistic particles (such as cosmic rays measured by either neutron monitors or muon detectors), the exact value of p has little effect on the simulation results. The separable solutions of § 2.2 depend on u/v, which in this case is nearly constant at $\approx u/c$, and shock encounters result in a fractional momentum increase that is independent of p. The grid spacings in the simulations were $\Delta\mu = 2/45$ and $\Delta z/\lambda = 0.05$, with $v\Delta t/\Delta z = 0.4\lambda$. (Recall that z refers to the distance from the shock along the magnetic field, and λ is the parallel mean free path.) Outer boundaries were placed at $\pm 8\lambda$ from the shock. A spectral index of 2.7 was assumed; the simulation results were found to be insensitive to this value. We allowed the simulations to evolve for a constant simulation time chosen to yield a typical peak-to-minimum anisotropy of a few percent in the near upstream region, in accord with observations (see, e.g., Nagashima et al. 1992). Results presented below are based on the simulated spatial and pitch-angle distribution of cosmic rays at this instant of time. There was very little difference in the results when comparing simulations evolved to a constant peak-to-minimum anisotropy.

In this work we do not expect to accurately model the Forbush decrease itself downstream of the shock, since we do not take into account the evolution of the shock as it moves outward, the presence of CME ejecta, etc. Nevertheless, we consider this a plausible model of the upstream precursors, because the distribution function upstream is mainly affected by a deficit of particles in the fresh plasma downstream and not as much by the detailed conditions there.

The numerical methods are based on those of Ruffolo (1999) and Nutaro, Riyavong, & Ruffolo (2001). One significant modification is that while Ruffolo (1999) assumed that pitch-angle changes at an oblique shock conserve the adiabatic invariant, $p_\perp^2/(2meB) \propto (1-\mu^2)/B$ (the magnetic moment), we now consider particle orbits as they cross the shock, using a transfer matrix to assign the distribution function to the appropriate μ- and z-cells after the shock encounter (D. Ruffolo et al. 2003, in preparation). In principle, the treatment of particle orbits should be more accurate than the assumption of conservation of the adiabatic invariant. In any case, we have found that results of the present work are essentially the same for both numerical treatments, for a variety of shock-field angles.

Note that, following Ng & Wong (1979), equation (1) is expressed in terms of F, the distribution function of particles in a magnetic flux tube. We present results in terms of the particle intensity j, where the two quantities are related by $F = 2\pi Aj$ and $A(z)$, the area of the flux tube, is inversely proportional to the magnetic field strength B. (The intensity j is in turn related to the phase-space density f by $j = p^2 f$.) We normalize the results so that j averaged over μ is unity at the far downstream boundary.

3. RESULTS

The numerical simulations yield the particle intensity j as a function of μ, the pitch-angle cosine in the local fluid frame, and z, the distance from the shock along the magnetic field in units of the mean free path λ. Figure 4 shows sample distributions for $\tan\theta_{Bn} = 4$, i.e., $\theta_{Bn} = 76°$ (recall that θ_{Bn} is the angle between upstream magnetic field lines and the shock normal). The upper panel is for $q = 0.5$, and

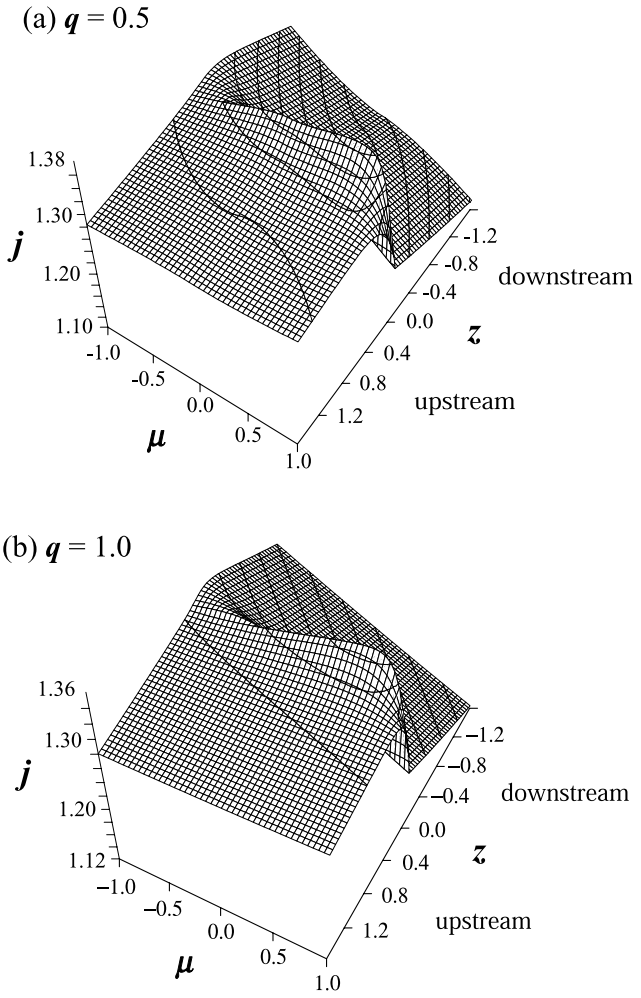

FIG. 4.—Intensity distribution, j, of Galactic cosmic rays as a function of μ and z (in units of λ) near an oblique shock with $\theta_{Bn} = 76^\circ$ for $q = (a)$ 0.5 and (b) 1.0.

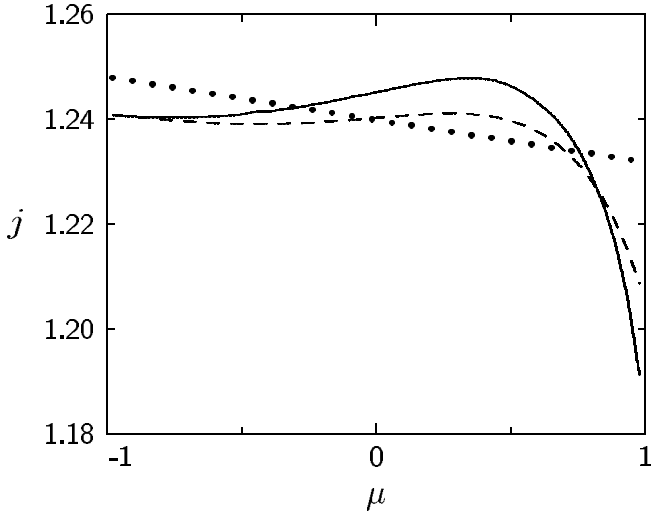

FIG. 5.—Simulated Galactic cosmic-ray intensity as a function of μ near an oblique interplanetary shock at $z = 0.025\lambda$ (*solid line*), 0.125λ (*dashed line*), and 1.575λ (*dotted line*) for $\theta_{Bn} = 76^\circ$ and $q = 1$.

the lower panel is for $q = 1.0$, close to the values appropriate for muon detectors and neutron monitors, respectively. The contours represent levels of equal particle intensity. For $\mu > 0$, particles are moving in the upstream direction (away from the Sun), and for $\mu < 0$ particles are moving downstream (toward the Sun).

In both panels, we see significant changes in the pitch-angle distribution near the shock (at $z = 0$). While particles moving with $\mu \approx -1$ flow from the upstream to the downstream side of the shock, particles with slightly higher μ are reflected, causing the increase in intensity for μ slightly greater than zero. Effectively, the shock is a barrier to particle propagation, damming the flow from upstream to downstream and causing the Forbush decrease downstream. The key difference between the results for $q = 0.5$ and 1 is the shape of the pitch-angle distribution, j versus μ, which is flattened near $\mu = 0$ in the former case because of enhanced scattering at a pitch angle of 90° (see § 2.1). At higher μ-values, close to $\mu = 1$, we are seeing particles that flow from downstream of the shock to the upstream side. Because of the deficit of particles downstream, there is a corresponding precursory decrease on the upstream side, for a narrow cone of directions around the magnetic field line, comprising the "loss cone." This is a distinctive anisotropy feature that is readily observable by ground-based neutron monitors and muon detectors.

At a given time, networks of detectors at Earth measure the directional distribution of Galactic cosmic rays, i.e., j as a function of μ at fixed z, corresponding to a slice through Figure 4. Such pitch-angle distributions are shown in Figure 5 for various distances from the shock, at $\tan\theta_{Bn} = 4$ and $q = 1$. At the earliest time, when the shock is greater than a mean free path away, an observer sees at most a diffusive anisotropy (*dotted line*) corresponding to the α_1 solution (see Fig. 3). As the shock moves closer to an intermediate distance (*dashed line*) or small distance (*solid line*), we see the α_2 solution with increasing strength, exhibiting both the loss cone decrease near $\mu = 1$ and the shock reflection increase just above $\mu = 0$. Thus, these precursors signal the imminent arrival of an interplanetary shock.

To be more precise, § 2.2 pointed out that the α_2 solution decays exponentially with increasing distance from the shock. Indeed, the steady state distribution function is a superposition of separable solutions (Fig. 3), each with a different decay length. Like Ruffolo (1999), we have found that the same separable solutions are recognizable in the results of time-dependent simulations, but with decay lengths that are somewhat different. Therefore, we have fitted our simulation results to determine these decay lengths numerically. In particular, the decay length of the α_2 feature can then be used as an indicator of the lead time for advance warning of the arrival of an interplanetary shock.

Since each separable solution has a nonzero contribution to the omnidirectional density of cosmic rays $\langle j\rangle_\mu$ as a function of z upstream of the shock, we can fit this to the sequence

$$\langle j\rangle_\mu = a_0 + a_1 e^{-z/\ell_1} + a_2 e^{-z/\ell_2} + \cdots , \qquad (8)$$

where a_i is the coefficient of the α_i solution and ℓ_i is the corresponding decay length. The first term in equation (8) corresponds to the solution far upstream, i.e., the quiet-time density of Galactic cosmic rays, the second term is a diffusive solution that decays over $\ell_1 = D/u$ from the shock, and

TABLE 2
ANGULAR WIDTH AND DECAY LENGTH OF LOSS CONE FEATURES

q	$\tan\theta_{Bn}$	θ_{Bn} (deg)	$\theta_{\rm HW}$ (deg)	ℓ (simulation)[a] (λ)	ℓ (steady state)[a] (λ)
0.1.....	0.1	5.71	45.1	0.11	0.239
	0.25	14.04	42.5	0.14	0.239
	0.5	26.56	32.8	0.19	0.239
	1.0	45.00	25.4	0.24	0.239
	4.0	75.96	24.8	0.25	0.238
0.5.....	0.1	5.71	49.3	0.08	0.195
	0.25	14.04	44.3	0.13	0.195
	0.5	26.56	33.4	0.17	0.195
	1.0	45.00	25.9	0.21	0.195
	4.0	75.96	24.8	0.23	0.194
1.0.....	0.1	5.71	57.2	0.05	0.137
	0.25	14.04	46.8	0.11	0.137
	0.5	26.56	34.7	0.14	0.137
	1.0	45.00	26.9	0.17	0.137
	4.0	75.96	24.8	0.21	0.137
1.5.....	0.1	5.71	68.3	0.03	0.073
	0.25	14.04	50.3	0.07	0.073
	0.5	26.56	37.1	0.09	0.073
	1.0	45.00	29.6	0.11	0.073
	4.0	75.96	25.0	0.17	0.073

[a] Decay length of the loss cone feature.

the higher order terms appear closer and closer to the shock. Here we fitted our simulation results up to the second term, which is sufficient for extracting ℓ_2, the decay length of the loss cone feature. Indeed, our simulations had insufficient spatial resolution to resolve higher order features.

Table 2 summarizes the decay length of loss cone features as derived from our simulations for varying q and θ_{Bn}, including both quasi-parallel and quasi-perpendicular shock configurations. Note that we do not expect the decay length from our time-dependent simulations to exactly correspond to the steady state result. In a steady state, ℓ/λ depends only on q and rather weakly on $|u_n|\sec\theta_{Bn}/v$. On the other hand, in more realistic time-dependent simulations it has a substantial variation with both q and θ_{Bn}. As shown in Figure 6*a*, the decay length (and hence the lead time in space weather forecasting) decreases substantially with increasing q, in qualitative agreement with the steady state theory.

We also see that the decay length is much longer for quasi-perpendicular shocks than for quasi-parallel shocks. This circumstance is rather fortunate, because loss cones from quasi-perpendicular shocks will generally provide less advance warning of shock arrival by virtue of the geometric relation $\Delta r = \Delta z\cos\theta_{Bn}$ (assuming radial shock propagation). The increase of ℓ/λ with θ_{Bn} partially counteracts this. Figure 6*b* plots as a function of q the ratio $\ell\cos\theta_{Bn}/\lambda$, which determines the lead time of a loss cone precursor in the case of radial propagation (see eq. [9]). There is less overall spread in this quantity than in ℓ/λ (Fig. 6*a*), and the shape of these curves evolves more smoothly with θ_{Bn}. (Note also that we estimate an uncertainty in the ℓ-values on the order of 10% and not less than 0.01λ.) We see that the intermediate shock-field angles provide the longest lead time for space weather forecasting.

Finally, our simulations can also address the angular width of the loss cone, which in principle can be observed by ground-based cosmic-ray detectors. Here the loss cone width is defined by the point at which the intensity decrease (relative to the omnidirectional intensity $\langle j\rangle_\mu$) has reached half its maximum value. In three dimensions, this indicates the half-width opening angle of the loss

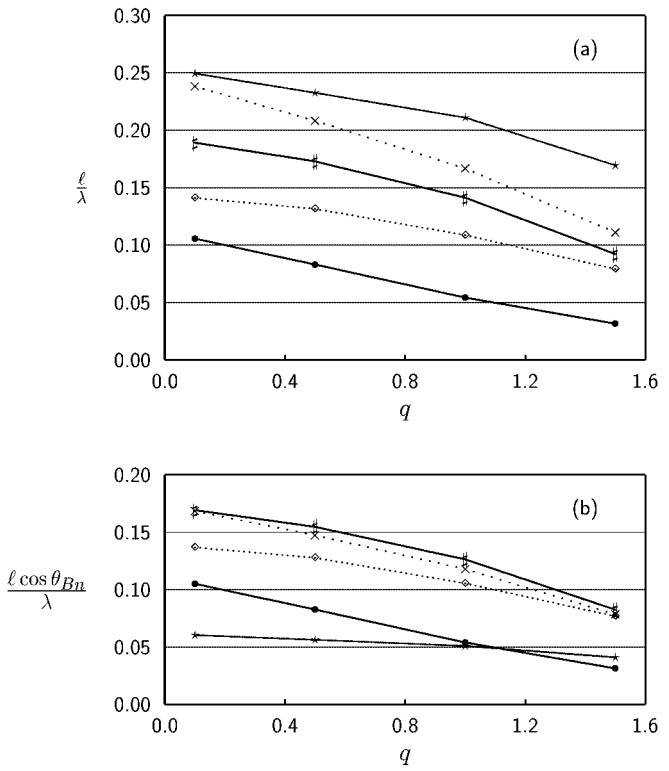

FIG. 6.—(*a*) Loss cone decay length, ℓ (in units of λ), as a function of q for shock-field angles $\theta_{Bn} = 5.^\circ7$ (*circles*), $14.^\circ0$ (*diamonds*), $26.^\circ6$ (*number signs*), $45.^\circ0$ (*crosses*), and $76.^\circ0$ (*stars*). (*b*) The quantity $\ell\cos\theta_{Bn}/\lambda$, which determines precursor lead time in the case of radial shock propagation, as a function of q for the same shock-field angles.

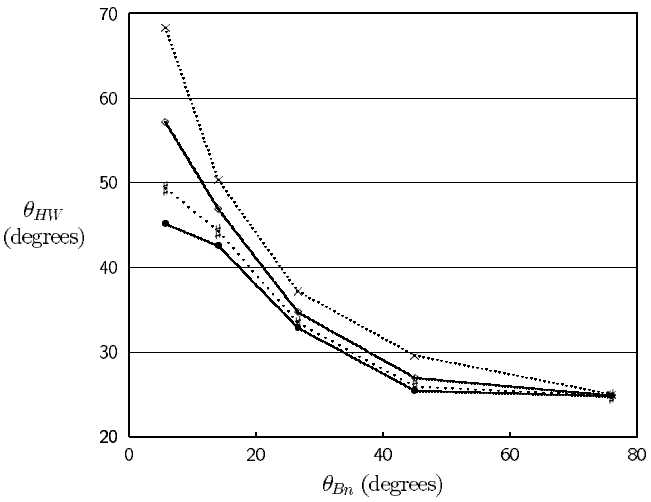

FIG. 7.—Loss cone opening angle, $\theta_{\rm HW}$, as a function of the shock-field angle θ_{Bn} for $q = 0.1$ (*circles*), 0.5 (*number signs*), 1.0 (*diamonds*), and 1.5 (*crosses*).

cone, and we denote it as $\theta_{\rm HW}$. The determination of loss cone width is made in the near upstream region, specifically $z = \lambda/40$. This quantity is also given in Table 2 for various values of q and θ_{Bn}. As shown in Figure 7, the loss cone opening angle tends to decrease with the shock-field angle. For a low shock-field angle (quasi-parallel shock), the width increases with increasing q, but the width tends to be independent of q for a high shock-field angle (quasi-perpendicular shock).

4. DISCUSSION

In this section, we use our results to estimate the expected lead time for loss cones observed by muon detectors and neutron monitors, i.e., the time of advance warning before the arrival of an interplanetary shock. Both detector types respond to a broad range of energies, with the median energy of response being ~60 GeV for a muon detector and ~17 GeV for a high-latitude neutron monitor. Shock interactions with ambient cosmic rays, however, disproportionately affect the particles of lower energy. The depth of a Forbush decrease, for instance, varies inversely with energy for the energies under consideration here (Morishita et al. 1990). From these considerations, we adopt 30 and 10 GeV, respectively, for the effective energies of cosmic rays measured by a muon detector and a neutron monitor when observing a loss cone.

Two important factors differentiate muon detectors and neutron monitors for purposes of estimating the expected loss cone decay length. First, the particles they detect have different scattering mean free paths. Second, and less obvious, the particles are resonant with different ranges of the turbulence spectrum corresponding to different spectral indices q, where q is the exponent of a presumed power-law spectrum varying with wavenumber k as $|k|^{-q}$.

From an analysis of the detailed shape of the cosmic-ray pitch-angle distribution measured by neutron monitors, Bieber & Pomerantz (1983) determined that a spectral index $q = 1.1$ and a mean free path $\lambda_\parallel = 0.5$ AU describe the data well for an effective cosmic-ray energy of 10 GeV. The mean free path is consistent with the value ~1 AU at slightly higher energy (17 GeV) obtained by analysis of cosmic-ray streaming and gradients (Chen & Bieber 1993).

The value $q = 1.1$ is reasonably consistent with the typical value $q \sim 1.2$ derived from direct measurement of the IMF power spectrum in the low-frequency regime of relevance to neutron monitor energies (Bieber et al. 1993). Further, it is consistent with current understanding of the turbulence power spectrum. Cosmic rays of 10 GeV are resonant with fluctuation scales near the turbulence correlation length, as illustrated in Figure 2. To compute a representative resonant wavenumber, we use $k_{\rm res} = (R_L \cos\theta)^{-1}$, with pitch angle $\theta = 45°$ and with the Larmor radius R_L computed for a 5 nT magnetic field. For the effective cosmic-ray energy measured by neutron monitors (indicated by n in Fig. 2), the resonant wavenumber almost exactly equals the inverse of the turbulence correlation length, $\lambda_c^{-1} \approx 3 \times 10^{-10}$ m^{-1}. At this length scale, the power spectrum is steepening from the comparatively shallow slope ($q \sim 0$–1) of the turbulence energy–containing range to the Kolmogoroff slope ($q = 5/3$) of the inertial range. Although the spectrum shown in the figure has a continually changing slope near the correlation scale, a value $q = 1.1$ is reasonable for comparison with our simulations, which assume a constant slope.

It has also been reported that a range of "$1/f$ noise" (i.e., $q = 1$) exists in low-frequency turbulence (Matthaeus & Goldstein 1982). Expressed in terms of the wavenumber, this range would be centered approximately on the correlation scale in Figure 2, $k = \lambda_c^{-1} \approx 3 \times 10^{-10}$ m^{-1}, and would extend for about a factor of 5 on either side of the correlation scale. This again supports using a value of q near unity for neutron monitor energies.

The mean free path at cosmic-ray energies appropriate for muon detectors is reported to be higher than that for neutron monitors (Hall, Duldig, & Humble 1997). This is in accord with the theoretical expectation that the mean free path λ should depend on particle rigidity P as $\lambda \propto P^{2-q}$. With $q = 1.1$, this implies a nearly linear relationship. Accordingly, we adopt a value of $\lambda = 1.5$ AU for muon detector measurements, which is simply 3 times the neutron monitor value.

Direct evidence for the value of q appropriate to muon detectors is lacking. However, based on the general characteristics of turbulence spectra discussed above and illustrated in Figure 2, we expect a smaller value of q than for neutron monitors. Estimates based on simple model spectra (see, e.g., Bieber et al. 1994) lead us to adopt $q = 0.5$ for muon detector energies.

The representative parameters for the two detector types are listed in Table 3. With q and $\lambda_\parallel$ known, we are now in a position to estimate the ratio $\ell/\lambda_\parallel$ from Figure 6. We use the curve for $\tan\theta_{Bn} = 1$, i.e., a shock normal angle of 45°. These ratios, along with the implied value of the decay length ℓ itself, are shown in the table. Finally, to convert the decay length to a lead time T that might be applicable to space weather forecasting, we assume a radially propagating shock, in which case T is given by

$$T = \frac{\ell \cos\theta_{Bn}}{V_s} , \qquad (9)$$

where V_s is the shock speed in Earth's rest frame. For purposes of illustration, we take $V_s = 600$ km s^{-1} and (as previously stated) $\theta_{Bn} = 45°$. Equation (9) presumes that

TABLE 3
ESTIMATED LOSS CONE LEAD TIMES

Detector Type	Representative Energy (GeV)	q	λ (AU)	ℓ/λ	ℓ (AU)	T (hr)
Neutron monitor.....	10	1.1	0.5	0.16	0.08	4
Muon detector	30	0.5	1.5	0.21	0.31	15

the loss cone will first be detectable exactly one decay length upstream, although in fact the exact distance will depend on other factors, such as the width and depth of the loss cone, as well as how complete the observing network's directional coverage is.

As shown in the last column of Table 3, our estimated lead time is 15 hr for muon detectors and 4 hr for neutron monitors. This is in good agreement with the observational results discussed in § 1 and illustrated in Figure 1. Typical lead times actually observed by muon detectors are indeed somewhat less than our estimate. However, the existing muon detector network has coverage only in the eastern hemisphere (Japan, Australia, and Antarctica). As noted by Munakata et al. (2000), the first detection of a loss cone by muon detectors often occurs when the detector network rotates into the sunward viewing direction. The loss cone may have been present prior to this, but it was unobserved owing to gaps in the muon detector network. (Fortunately, sky coverage by the muon detector network is improving thanks to the installation and planned expansion of a muon detector in São Martinho, Brazil. See Munakata et al. 2001.)

Next, let us consider how observations of individual loss cone precursors can in principle indicate the shock arrival time on a case-by-case basis. In Figure 7, we see that for large field-shock normal angles θ_{Bn}, i.e., for quasi-perpendicular shocks, the loss cone opening angle $\theta_{\rm HW}$ is nearly independent of q. This is even approximately true for θ_{Bn} as low as $\approx 15^\circ$. Therefore, an observational measurement of $\theta_{\rm HW}$ gives a fairly good determination of θ_{Bn}. (Note, however, that for a parallel shock there should not be a loss cone precursor, as there is no shock reflection or change in pitch angle as particles cross the shock. For nearly parallel shocks the loss cone is not very deep and may be difficult to observe.) At the very least, there is a robust indication that for a wide loss cone opening angle ($\gtrsim 45^\circ$) the shock is quasi-parallel and that for a narrow loss cone opening angle ($\lesssim 30^\circ$) the shock is quasi-perpendicular.

Observational indications of shock-field angles are of interest in and of themselves; furthermore, they provide a means to estimate the lead time before the shock arrival. If we can estimate the shock-field angle and q, then we can obtain ℓ/λ from Figure 6. Assuming for simplicity that the shock normal is in the radial direction, we can estimate the lead time from equation (9). Taking measurement uncertainties into account, this technique can at least give a qualitative indication of whether the shock arrival should be imminent or delayed. With further observations, or testing on historical data, this indication could be calibrated to give quantitative forecasts of the shock arrival time.

5. CONCLUSIONS

Observed precursors to Forbush decreases can be explained in a mathematical framework of cosmic-ray pitch-angle transport near an oblique, plane-parallel shock. Loss cone decreases and shock reflection increases should occur in tandem, corresponding to the same separable solution of the transport equation. Numerical simulations of cosmic-ray interactions with a CME shock have been performed for various shock-field angles and various values of q, the power-law index of magnetic turbulence. We point out that different values of q are appropriate for cosmic rays of different energy ranges and show that loss cone precursors to Forbush decreases should typically be detectable by neutron monitors about 4 hr prior to shock arrival and by muon detectors about 15 hr prior to shock arrival. The results are consistent with observational surveys and suggest that ground-based cosmic-ray detectors can play a useful role in space weather forecasting.

In addition, our work has shown that the width of a precursor loss cone provides a prediction of whether the approaching shock is quasi-parallel or quasi-perpendicular. Quasi-perpendicular shocks produce loss cones with opening angles of $\sim 25^\circ$, whereas quasi-parallel shocks have loss cones with opening angles of $\sim 50^\circ$. This removes another unknown in the estimation of the lead time and implies that loss cone measurements can in principle provide a quantitative indication of the time when an interplanetary shock will arrive at Earth.

K. L. and D. R. greatly appreciate the hospitality of the Bartol Research Institute, University of Delaware, where this work was conceived. This work was partially supported by a Basic Research Grant and a Royal Golden Jubilee Fellowship from the Thailand Research Fund, NSF grants ATM 00-00315 and ATM 02-07196, and NASA grant NAG 5-8134.

REFERENCES

Belov, A. V., Bieber, J. W., Eroshenko, E. A., Evenson, P., Pyle, R., & Yanke, V. G. 2001, Proc. 27th Int. Cosmic-Ray Conf. (Hamburg), 9, 3507
Belov, A. V., Dorman, L. I., Eroshenko, E. A., Iucci, N., Villoresi, G., & Yanke, V. G. 1995, Proc. 24th Int. Cosmic-Ray Conf. (Rome), 4, 888
Bieber, J. W., Chen, J., Matthaeus, W. H., Smith, C. W., & Pomerantz, M. A. 1993, J. Geophys. Res., 98, 3585
Bieber, J. W., & Evenson, P. 1998, Geophys. Res. Lett., 25, 2955
Bieber, J. W., Matthaeus, W. H., Smith, C. W., Wanner, W., Kallenrode, M.-B., & Wibberenz, G. 1994, ApJ, 420, 294
Bieber, J. W., & Pomerantz, M. A. 1983, Geophys. Res. Lett., 10, 920
Cane, H. V. 1993, J. Geophys. Res., 98, 3509
Cane, H. V., Richardson, I. G., & von Rosenvinge, T. T. 1996, J. Geophys. Res., 101, 21561
Cane, H. V., Richardson, I. G., von Rosenvinge, T. T., & Wibberenz, G. 1994, J. Geophys. Res., 99, 21429
Chen, J., & Bieber, J. W. 1993, ApJ, 405, 375
de Hoffmann, F., & Teller, E. 1950, Phys. Rev., 80, 692
Dorman, L. I., Iucci, N., & Villoresi, G. 1995, Proc. 24th Int. Cosmic-Ray Conf. (Rome), 4, 892

Duggal, S. P., & Pomerantz, M. A. 1976, J. Geophys. Res., 81, 5032
Gosling, J. T., Bame, S. J., McComas, D. J., & Phillips, J. L. 1990, Geophys. Res. Lett., 17, 901
Hall, D. L., Duldig, M. L., & Humble, J. E. 1997, ApJ, 482, 1038
Jokipii, J. R. 1966, ApJ, 146, 480
———. 1971, Rev. Geophys. Space Phys., 9, 27
Kirk, J. G. 1988, ApJ, 324, 557
Kirk, J. G., & Schneider, P. 1987, ApJ, 315, 425
Krymskii, G. F. 1977, Soviet Phys.–Dokl., 22, 327
Kudela, K., Flückiger, E. O., Langer, R., & Bobik, P. 1997, Proc. 25th Int. Cosmic-Ray Conf. (Durban), 2, 425
Kudela, K., Venkatesan, D., Flückiger, E. O., Langer, R., Martin, I. M., Slivka, M., & Graumann, H. 1995, Proc. 24th Int. Cosmic-Ray Conf. (Rome), 4, 928
Lockwood, J. A. 1971, Space Sci. Rev., 12, 658
Matthaeus, W. H., & Goldstein, M. L. 1982, J. Geophys. Res., 87, 6011
Morishita, I., Nagashima, K., Sakakibara, S., & Munakata, K. 1990, Proc. 21st Int. Cosmic-Ray Conf. (Adelaide), 6, 217
Morishita, I., et al. 1997, Proc. 25th Int. Cosmic-Ray Conf. (Durban), 1, 405
Munakata, K., et al. 2000, J. Geophys. Res., 105, 27457
———. 2001, Proc. 27th Int. Cosmic-Ray Conf. (Hamburg), 9, 3494
Nagashima, K., Fujimoto, K., & Morishita, I. 1994, J. Geophys. Res., 99, 21419
Nagashima, K., Fujimoto, K., Sakakibara, S., Morishita, I., & Tatsuoka, R. 1992, Planet. Space Sci., 40, 1109
Ng, C. K., & Wong, K.-Y. 1979, Proc. 16th Int. Cosmic-Ray Conf. (Kyoto), 5, 252
Nutaro, T., Riyavong, S., & Ruffolo, D. 2001, Comput. Phys. Commun., 134, 209
Ruffolo, D. 1995, ApJ, 442, 861
———. 1999, ApJ, 515, 787
Ruffolo, D., Bieber, J. W., Evenson, P., & Pyle, R. 1999, Proc. 26th Int. Cosmic-Ray Conf. (Salt Lake City), 6, 440